Biological, Medical Devices, and Systems

High-throughput Measurement of Single-cell Growth Rates using Serial Microfluidic Mass Sensor Arrays

N. Cermak, S. Olcum, F. F. Delgado, S. C. Wasserman, K. R. Payer, S. M. Knudsen, R. J. Kimmerling, M. M. Stevens, M. Ogawa, V. Agache, F. Baléras, S. R. Manalis
Sponsorship: NIH, AFOSR

Methods to rapidly assess cell growth would be useful for many applications, including drug susceptibility testing, but current technologies have limited sensitivity or throughput. Here we present an approach to precisely and rapidly measure growth rates of many individual cells simultaneously.

We flow cells in suspension through a microfluidic channel with 10–12 resonant mass sensors distributed along its length, weighing each cell repeatedly over the 4–20 min it spends in the channel (Figures 1, 2). Because multiple cells traverse the channel at the same time, we obtain growth rates for >60 cells/h with a resolution of 0.2 pg/h for mammalian cells and 0.02 pg/h for bacteria. We measure the growth of single lymphocytic cells, mouse and human T cells, primary human leukemia cells, yeast, Escherichia coli and Enterococcus faecalis. Our system reveals subpopulations of cells with divergent growth kinetics and enables assessment of cellular responses to antibiotics and antimicrobial peptides within minutes.

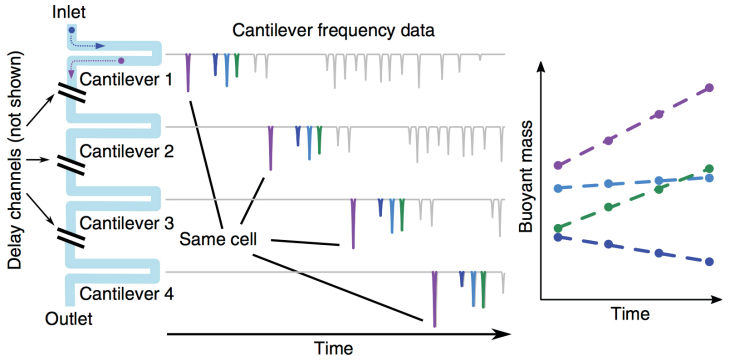

▲ Figure 1: Design and implementation of the serial SMR array. Simulated data showing frequency peaks originating from single cells flowing through a series of SMRs (cantilever mass sensors) separated by delay channels. Cells grow as they traverse the array. After frequency peaks originating from the same cell are grouped, that cell's mass accumulation rate can be obtained by regressing its buoyant mass versus time. Because many cells can traverse the array simultaneously, this device can achieve much higher throughput than a single SMR device.

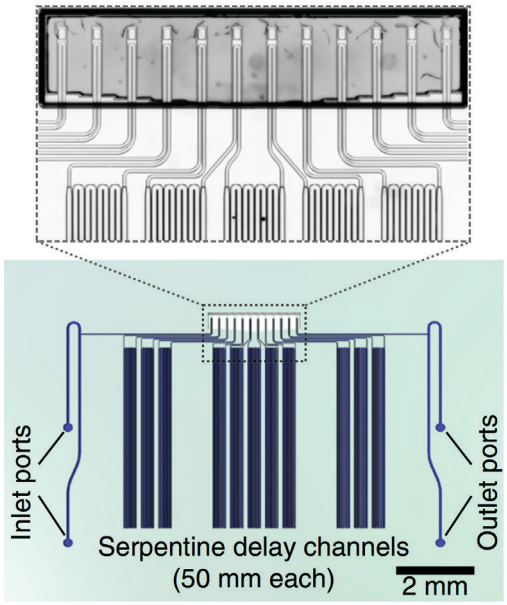

▲ Figure 2: Rendering of a large-channel serial SMR array device showing delay channels and the cantilevers (magnified in inset micrograph).

FURTHER READING

- M. M. Stevens, C. L. Maire, N. Chou, M. Murakami, D. Knoff, Y. Kikuchi, R. J. Kimmerling, H. Liu, S. Haidar, N. L. Calistri, N. Cermak, S. Olcum, N. Cordero, A. Idbaih, P. Y. Wen, D. M. Weinstock, K. L. Ligon, and S. R. Manalis, "Drug Sensitivity of Single Cancer Cells is Predicted by Changes in Mass Accumulation Rate," *Nature Biotechnology*, vol. 34, pp. 1161-1167, 2016.
- N. Cermak, S. Olcum, F. F. Delgado, S. C. Wasserman, K. R. Payer, M. Murakami, S. M. Knudsen, R. J. Kimmerling, M. M. Stevens, Y. Kikuchi, A. Sandikci, M. Ogawa, V. Agache, F. Baléras, D. M. Weinstock, and S. R. Manalis., "High-throughput Single-cell Growth Measurements via Serial Microfluidic Mass Sensor Arrays," *Nature Biotechnology*, vol. 34, pp. 1052-1059, 2016.

Iso-dielectric Separation of Cells and Particles

J. Lee, D.-H. Lee, J. Voldman
Sponsorship: NIH, Korea Foundation for Advanced Studies

The development of new techniques to separate and characterize cells with high throughput has been essential to many of the advances in biology and biotechnology over the past few decades. We are developing a novel method for the simultaneous separation and characterization of cells based upon their electrical properties. This method, iso-dielectric separation (IDS), uses dielectrophoresis (DEP, the force on a polarizable object) and a medium with spatially varying conductivity to sort electrically distinct cells while measuring their effective conductivity (Figure 1). It is similar to iso-electric focusing, except that it uses DEP instead of electrophoresis to concentrate cells and particles to the region in a conductivity gradient where their polarization charge vanishes [Figure 1].

Sepsis is an uncontrolled activation of the immune system that causes an excessive inflammatory response. There is an unmet need to develop tools to monitor sepsis progression, which occurs quickly and provides few clues to indicate if treatment is effective. Previously, we have found the electrical profile of leukocytes changes with activation state, and we have applied IDS to characterize the electrical profile of leukocytes for monitor sepsis. After working with neutrophils, we also found that IDS can be used to distinguish different types of leukocytes having different dielectric properties. As Figure 2 suggests, once cell properties such as size, permittivity and conductivity of each part change, Clausius-Mossotti (CM) factor changes and it explains the reason why we can distinguish different types of cells in IDS. We could distinguish neutrophils and T-cells (the majority of lymphocytes) at the frequency of 5 MHz and the area under ROC curve was 0.8473. To advance the automation of the system and reduction sample preparation for clinical deployment, we could integrate the upstream separator such as inertial microfluidic sorter for removal of red blood cells (RBC) from the patient's blood samples. It might be possible to monitor sepsis from patients in pseudo-real time.

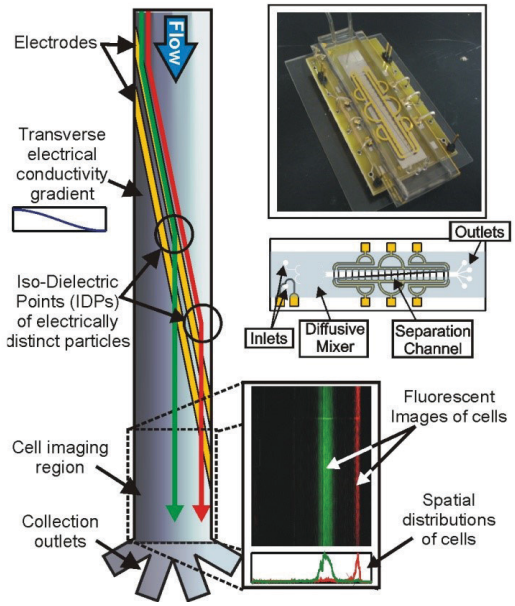

▲ Figure 1: Iso-dielectric separation (IDS) microfluidic device used to measure electrical properties of the cells. The spatial conductivity gradient makes cells with different electrical properties pass through the electrodes at different positions (isodielectric point - IDP).

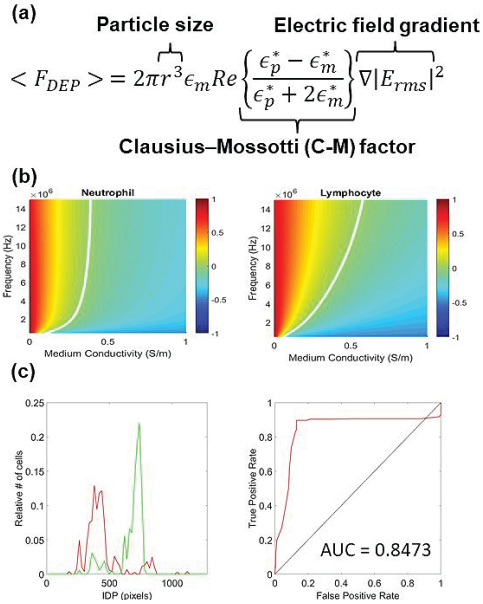

▲ Figure 2: Simulation and experiment results of IDS with neutrophils and lymphocytes (T-cells, in experiments). (a) DEP equation showing the relationship between the force and Clausius-Mossotti (C-M) factor. (b) Clausius-Mossotti (C-M) factor simulation results of neutrophil (left) and lymphocyte (right). (c) IDS profile of neutrophils (red) and T-cells (green), and corresponding ROC curve (right).

FURTHER READING

- J. L. Prieto, H. W. Su, H. W. Hou, M. P. Vera, B. D. Levy, R. M. Baron, J. Han, and J. Voldman, "Monitoring Sepsis using Electrical Cell Profiling," *Lab on a Chip,* vol. 16, pp. 4239-4468, 2016.
- H. W. Su, J. L. Prieto, and J. Voldman, "Rapid Dielectrophoretic Characterization of Single Cells using the Dielectrophoretic Spring," *Lab on a Chip,* vol. 13, pp. 4109-4117, 2013.
- M.D. Vahey and J. Voldman, "An Equilibrium Method for Continuous-flow Cell Sorting using Dielectrophoresis," *Analytical Chemistry,* vol. 80, no. 9, pp. 3135-3143, 2008.

Microfluidic Electronic Detection of Protein Biomarkers

D. Wu, J. Voldman
Sponsorship: Analog Devices, Inc.

Traditional blood tests are performed in centralized laboratories by trained technicians and need days to deliver results. The need of ~mL blood sample also makes it challenging to apply the traditional tests to premies or even newborns. We are developing a miniaturized microfluidic electronic biosensor, which gives immediate results (within 30 minutes) and needs ~µL blood, for diagnosis of neonate sepsis. To achieve this goal, we developed portable PCB-based multiplexed amperometry circuitry and a bead-based electronic enzyme-linked immunosorbent assay. Combining the circuitry and bead-based assay, we have demonstrated measurement of human interleukin-6, a potential neonatal sepsis biomarkers, in serum with clinically relevant limit of detection (e.g., < 40pg/ml).

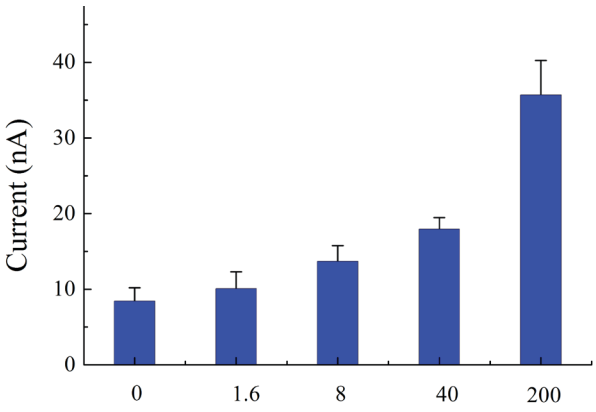

▲ Figure 2: Assay of IL-6 in serum.

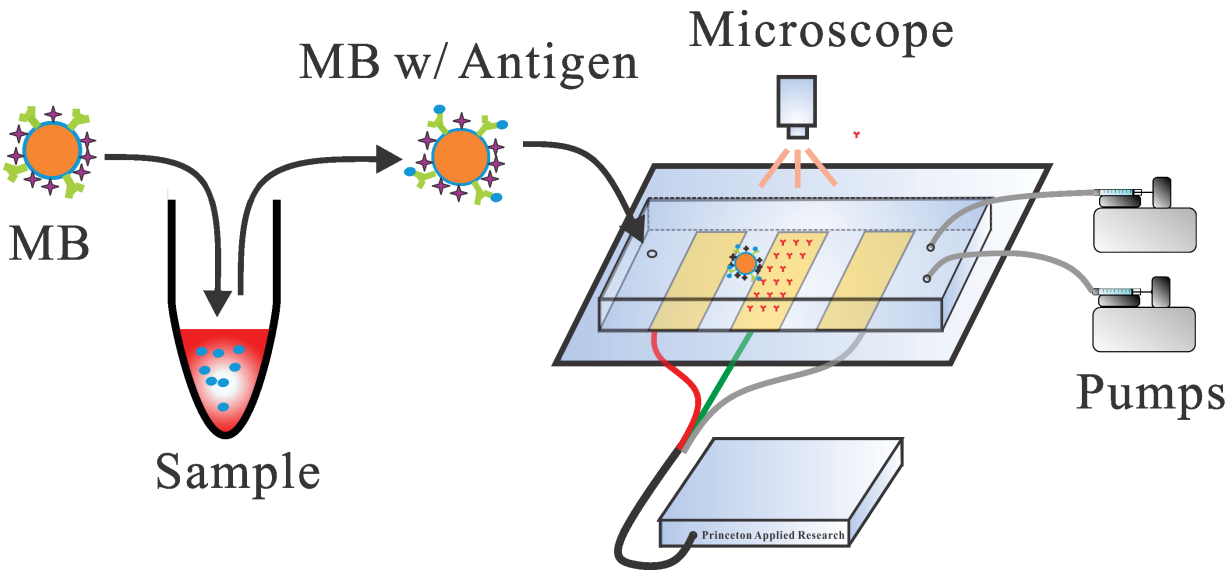

▲ Figure 1: Schematic of the bead-based electronic enzyme-linked immunosorbent assay (ELISA).

Continuous Biomanufacturing Using Micro/nanofluidics

T. Kwon, S. H. Ko, J.-F. P. Hamel, J. Han
Sponsorship: SMART Centre BioSyM IRG, DARPA, Samsung Scholarship

Continuous biomanufacturing is a growing trend in the biopharmaceutical industry because it can reduce manufacturing cost and increase product quality. Ideas from micro/nanofluidics can be employed in all aspects of continuous biomanufacturing to enhance the overall productivity as well as the efficacy and safety of the final products.

First, we introduce a novel cell retention device based on inertial sorting for perfusion culture (Figure 1). The cell retention device maintains cells in the bioreactor and removes biologics and metabolites. Hollow fiber membrane is commonly used in the biopharmaceutical industry. However, it has challenges, such as membrane clogging/fouling, low product recovery, and inability to remove dead cells. In this context, we developed a membrane-less microfluidic cell retention device and demonstrated perfusion culture of high-concentration mammalian cells producing monoclonal antibodies for >3 weeks with high product recovery (>99%).

Second, we present a nanofluidic system for continuous-flow, multi-variate (purity, bioactivity, and protein folding) protein analysis for real-time critical quality assessments (Figure 2). This size-based nanofluidic system can complement the existing bench-type conventional analytical tools, such size exclusion chromatography and gel electrophoresis, to meet quality assurance requirements of current and future biomanufacturing systems. We demonstrated rapid purity and bioactivity monitoring of protein drugs, such as hGH, IFN-alfa-2b, and G-CSF, using the nanofluidic system.

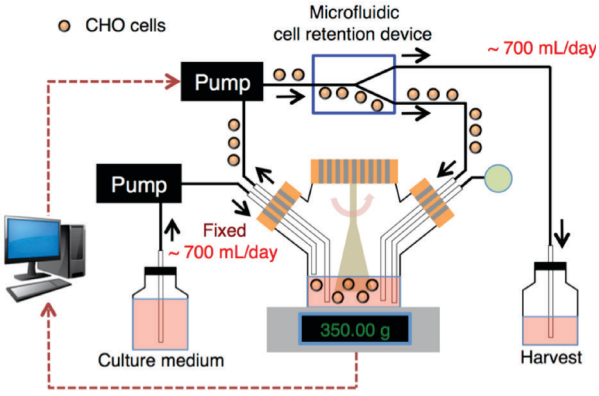

▲ Figure 1: System schematic of perfusion culture using a microfluidic cell retention device. The Chinese Hamster Ovary (CHO) cells are maintained in a bioreactor, and monoclonal antibodies produced from these cells are collected in a harvest bottle.

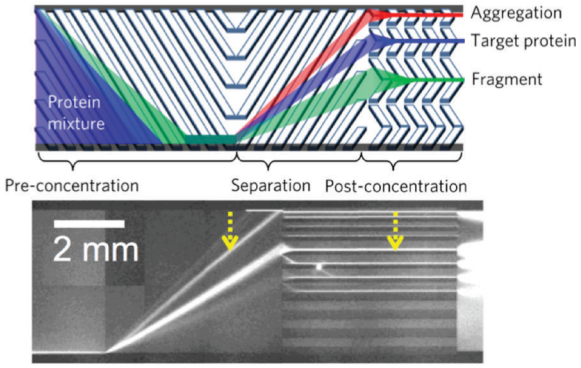

▲ Figure 2: Nanofluidic system for multi-variate protein analysis for real-time critical quality assessments. For example, it can monitor purity of Interferon alfa-2b biologic drugs.

FURTHER READING

- T. Kwon, H. Prentice, J. D. Oliveira, N. Madziva, M. E. Warkiani, J.-F. P. Hamel, and J. Han, "Microfluidic Cell Retention Device for Perfusion of Mammalian Suspension Culture," *Scientific Reports*, vol. 7, pp. 6703, 2017.
- T. Kwon, R. Yao, J.-F. P. Hamel, and J. Han, "High-density Perfusion Culture of Suspended Mammalian Cells and Continuous Removal of Cell Debris and Smaller Non-viable Cells using Inertial Microfluidics," *Proceedings of 21st International Conference on Miniaturized Systems for Chemistry and Life Sciences (MicroTAS)*, pp. 818-819, 2017.
- S. H. Ko, D. Chandra, W. Ouyang, T. Kwon, P. Karande, and J. Han, "Nanofluidic Device for Continuous Multiparameter Quality Assurance of Biologics," *Nature Nanotechnology*, vol. 12, pp. 804-812, 2017.

Ion Concentration Polarization Desalination using Return Flow System

J. Yoon, J. Han
Sponsorship: Korea Foundation for Advanced Studies

While the conventional electrodialysis (ED) relies on bipolar ion conduction employing two ion exchange membranes, anion exchange membrane (AEM) and cation exchange membrane (CEM), our group has proposed unipolar ion conduction, so-called ion concentration polarization (ICP) desalination, employing only CEM to enhance energy efficiency. Because chloride ion, the majority salt in nature, has faster diffusivity than sodium ion, ICP desalination theoretically has a current utilization (CU) of 1.2, but the ED has only that of 1. To facilitate the ICP desalination, our group has developed series of technology from Bifurcate ICP system to Trifurcate ICP (Tri-ICP) system. Here, we have developed a return flow (RF-ICP) desalination system with a newly designed flow path for improving energy efficiency.

Figure 1 shows a schematic of RF-ICP desalination system, which has three channels separated by two nano-porous membranes. The three channels consist of a concentrate channel on the anodic side, a diluate channel on the cathodic side, and an intermediate channel in between. A feed solution flows through the inlet of intermediate channel with the highest pressure and flows through the outlet of both side channels with the lowest pressure. As the feed solution flows through the channels, a portion of the feed solution flows through the porous membrane (Por-flow) due to the pressure difference. The Por-flows facilitate two types of flow barriers, a suppressor for a chaotic electroconvection in the diluate stream and a preventer for a salt leakage from the concentrate stream. The remaining solution returns at the end of channel (RF-flow) and induces the effect of sweeping a mass on the CEM surfaces by shear stress.

We demonstrate that the developed RF-ICP system reduces a power consumption compared to the previously developed Tri-ICP system. Also, the RF-ICP system showed symmetrical product concentrations between diluate and concentration (data not shown), and the recovery rate increased to 50% compared to the Tri-ICP system, which was 25%. To improve the performance of RF-ICP system, more optimized system would be developed by various operating controls for recovery rate increase or spacer designs for energy efficiency increase.

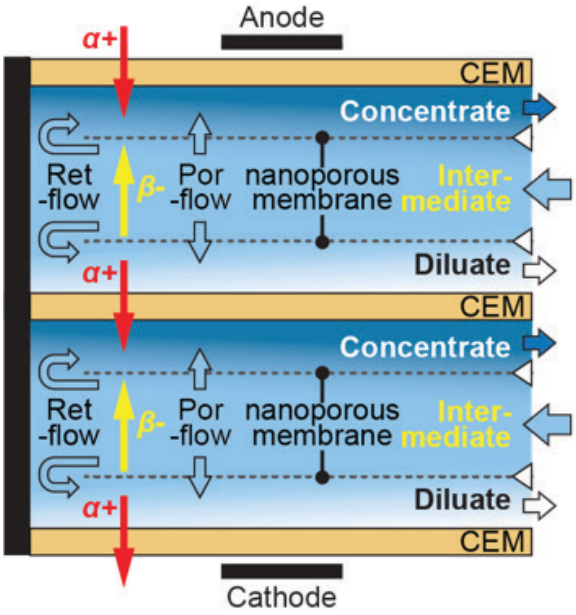

▲ Figure 1: Schematic illustration of ion transport and flow in RF-ICP desalination. Red and yellow arrows indicate the movement of cation λ+ and anion β− by electric field, respectively.

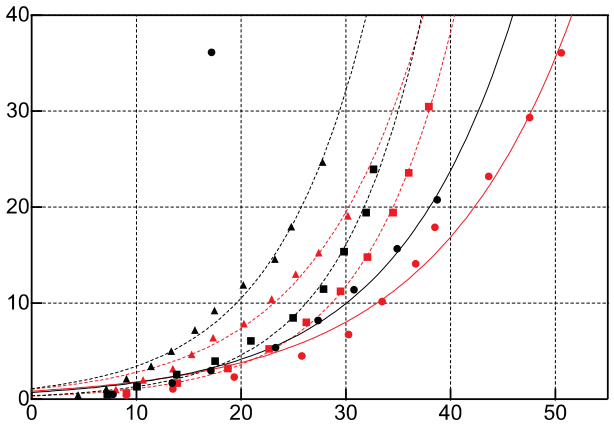

▲ Figure 2: Power consumption to achieve salt removal ratios with various flow velocities (1.5–3.0 mm/s).

FURTHER READING

- B. Kim, H. Kwon, S. H. Ko, G. Lim, and J. Han, "Partial Desalination of Hypersaline Brine by Lab-scale Ion Concentration Polarization Device," *Desalination*, 2017.
- R. Kwak, V. S. Pham, B. Kim, L. Chen, and J. Han, "Enhanced Salt Removal by Unipolar Ion Conduction in Ion Concentration Polarization Desalination," *Sci Rep.* 2016.
- B. Kim, R. Kwak, H. J. Kwon, et al., "Purification of High Salinity Brine by Multi-stage Ion Concentration Polarization Desalination," *Sci Rep.*, 2016.

A Printed Microfluidic Device for the Evaluation of Immunotherapy Efficacy

A. L. Beckwith, J. T. Borenstein, L. F. Velásquez-García
Sponsorship: Draper

Inherent challenges in device fabrication have impeded the widespread adoption of microfluidic technologies in the clinical setting. Additive manufacturing could address the constraints associated with traditional microfabrication, enabling greater microfluidic design complexity, fabrication simplification (e.g., removal of alignment and bonding process steps), manufacturing scalability, and rapid and inexpensive design iterations.

We have fabricated an entirely 3-D-printed microfluidic platform enabling the modeling of interactions between tumors and immune cells, providing a microenvironment for testing immunotherapy treatment efficacy. The monolithic platform allows for real-time analysis of interactions between a resected tumor fragment and resident or circulating lymphocytes in the presence of immunotherapy agents. Our high-resolution, non-cytotoxic, transparent device monolithically integrates a variety of microfluidic components into a single chip, greatly simplifying device operation when compared to traditionally-fabricated microfluidic systems. Human tumor fragments can be kept alive within the device. In addition, the tumor fragment within the device can be imaged with single-cell resolution using confocal fluorescence microscopy.

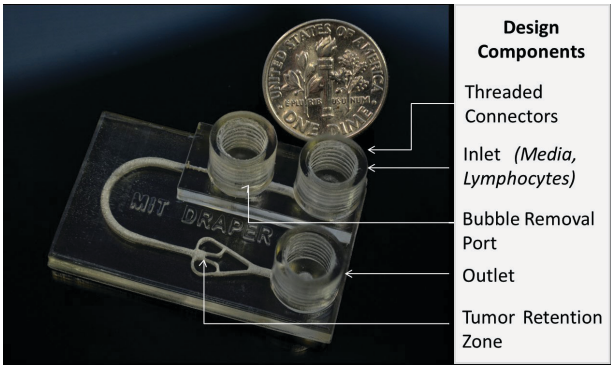

▲ Figure 1: An optical picture of a 3-D-printed, transparent, non-cytotoxic microfluidic platform for analysis of the efficacy of immunotherapy, with features labeled.

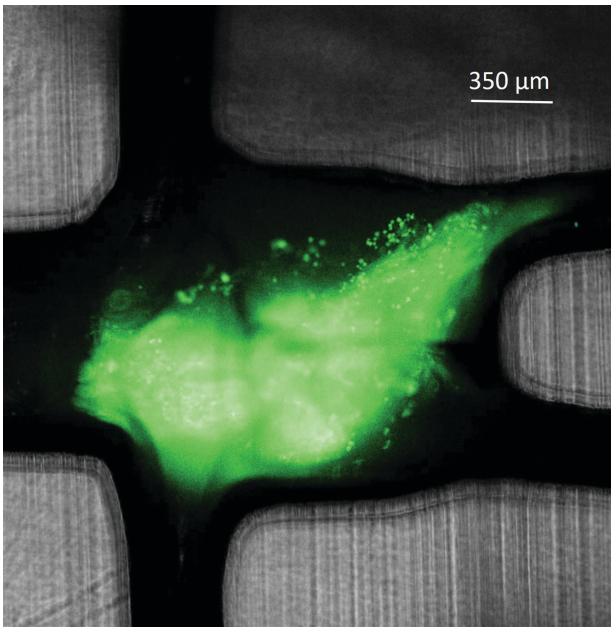

▲ Figure 2: Overlaid bright-field and fluorescence images enable visualization of device geometries in addition to the stained tumor fragment. Single cells are visible.

FURTHER READING

- Z. Sun and L. F. Velásquez-García, "Monolithic FFF Printed, Biodegradable, Biocompatible, Dielectric–conductive Microsystems," *J. of Microelectromechanical Systems*, vol. 26, no. 6, pp. 1356 – 1370, Dec. 2017.
- E. García-López, D. Olvera-Trejo, and L. F. Velásquez-García, "3-D Printed Multiplexed Electrospinning Sources for Large-scale Production of Aligned Nanofiber Mats with Small Diameter Spread," *Nanotechnology*, vol. 28, no. 42, pp. 425302, Oct. 2017.
- D. Olvera-Trejo and L. F. Velásquez-García, "Additively Manufactured MEMS Multiplexed Coaxial Electrospray Sources for High-Throughput, Uniform Generation of Core-shell Microparticles," *Lab on a Chip*, vol. 16, no. 21, pp. 4121 – 4132, Nov. 2016.

Biocompatible Dielectric-conductive Microsystems Monolithically 3-D Printed via Polymer Extrusion

Z. M. Sun, L. F. Velásquez-García

Additive manufacturing (AM), i.e., the layer-by-layer construction of devices using a computer-aided design (CAD) file, has been recently explored as a manufacturing toolbox for MEMS. The demonstration of monolithic multi-material devices in 3-D printed MEMS has the potential to implement better, more complex, and more capable microsystems at a small fraction of the time and cost typically associated with semiconductor cleanroom microfabrication. Fused filament fabrication (FFF) is an AM technique based on extrusion of thermoplastic polymers that is arguably the simplest and cheapest commercial 3-D printing technology available.

Here, we report additively manufactured monolithic microsystems composed of conductive and dielectric layers using an FFF dual extruder 3-D printer. The base material is a biocompatible polymer, polylactic acid (PLA), which can be doped with micro/nanoparticles to become electrically conductive. Characterization of the printing technology demonstrates close resemblance between CAD files and printed objects, generation of watertight microchannels, high-vacuum compatibility, and non-cytotoxicity. A large (~23) piezoresistive gauge factor was measured for a certain graphite-doped conductive PLA, suggesting its utility to implement 3-D printed strain transducers via FFF. Multiplexed electrohydrodynamic liquid ionizers (Figure 1) with integrated extractor electrode and threaded microfluidic port were also demonstrated. The per-emitter current vs. per-emitter flowrate characteristic shows a power dependence with 0.6 coefficient (Figure 2), close to the square-root dependence predicted by de la Mora's law for the cone-jet emission mode.

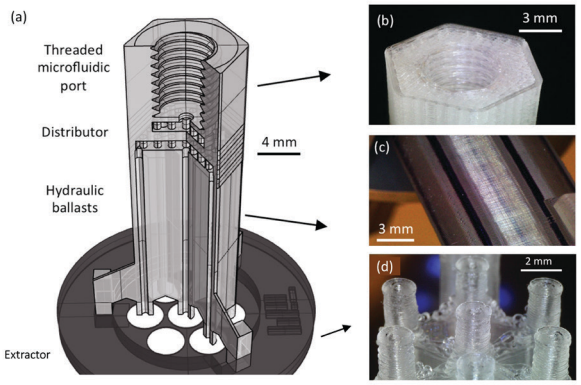

▲ Figure 1: CAD schematic and selected close-up views of FFF-printed 7-emitter electrospray array with hydraulics made of dielectric PLA and extractor electrode made of graphite-doped conductive PLA.

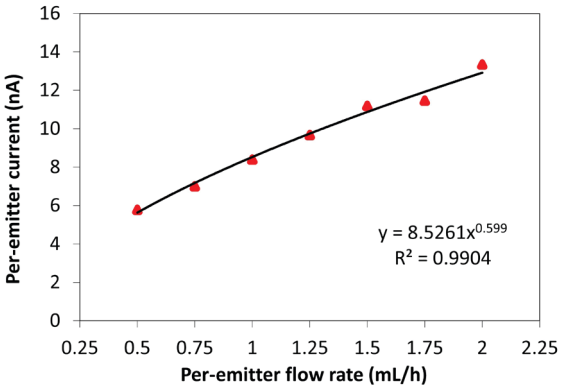

▲ Figure 2: Per-emitter current vs. flow rate characteristic for a fully-printed 7-emitter array with integrated extractor electrode and microfluidic port.

FURTHER READING

- Z. Sun and L. F. Velásquez-García, "Monolithic FFF Printed, Biodegradable, Biocompatible, Dielectric–conductive Microsystems," *J. Microelectromechanical Systems*, vol. 26, no. 6, pp. 1356 – 1370, Dec. 2017.
- D. Olvera-Trejo and L. F. Velásquez-García, "Additively Manufactured MEMS Multiplexed Coaxial Electrospray Sources for High-throughput, Uniform Generation of Core-shell Microparticles," *Lab on a Chip*, vol. 16, no. 21, pp. 4121 – 4132, Nov. 2016.
- L. F. Velásquez-García "SLA 3-D-Printed Arrays of Miniaturized, Internally-fed, Polymer Electrospray Emitters," *J. Microelectromechanical Systems*, vol. 24, no. 6, pp. 2117 - 2127, Dec. 2015.

Mini Continuous Stirred Tank Reactors (mini-CSTR) for Cell and Tissue Culture Applications

G. Trujillo-de Santiago, R. Hernández-Medina, C. del Toro-Runzer, C. Buenrostro-Mendoza, S. Gallardo, I. Anaya, E. González-González, A. Valverde, C. A. Rodríguez-González, Y. S. Zhang, M. M. Alvarez.
Sponsorship: MIT-Tecnológico de Monterrey Nanotechnology Program

An ideal cell culture system will provide a well-controlled, homogeneous, and steady environment for cells and tissues. For instance, well-controlled steady states would greatly benefit organ-on-chip experiments, stem cell culture, and tissue propagation (among other relevant biomedical applications). At present, no continuously stirred mini-reactors are commercially available for lab-scale culture applications.

We are developing simple, low-cost, and user-friendly miniaturized continuously stirred tank reactors (CSTRs) for biomedical and biotechnological agitations. These well-mixed mini-CSTRs will enable cost-efficient continuous culture at small scales. We cast Polydimethylsiloxane (PDMS) casting on poly(methyl-methacrylate) molds, or directly use high resolution 3-D-printing, to fabricate these CSTRs and an Arduino platform to measure and control key parameters, such as agitation, temperature, and pressure, in small portable incubators (Figure 1). Nutrients are fed by syringe pumps, and well-controlled low-speed (benign) agitation is provided by a custom-made magnetic system. Since the reactor behaves as a well-mixed reservoir, all bulk-liquid concentrations can be measured at the outlet stream, thereby greatly reducing the need for intrusive instrumentation. We are currently validating the use of this culture platform in two model applications: (a) the extended culture of breast cancer spheroids, and (b) the culture of Chinese Hamster Ovary Cells (the warhorse for biopharmaceutical production) for continuous production of biopharmaceutical compounds (Figure 2).

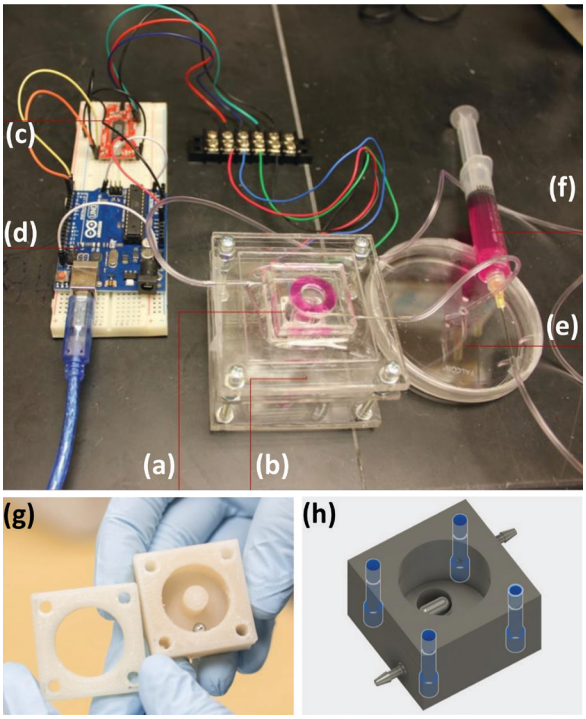

▲ Figure 1: Mini-CSTR controlled by Arduino: Complete setup of the system including a PDMS miniCSTR (a), stepper motor support (b), stepper motor driver (c), Arduino microcontroller (d), container for spent media (e), and fresh media (f). 3-D-printed mini-CSTR (first generation, g), and (second generation, h).

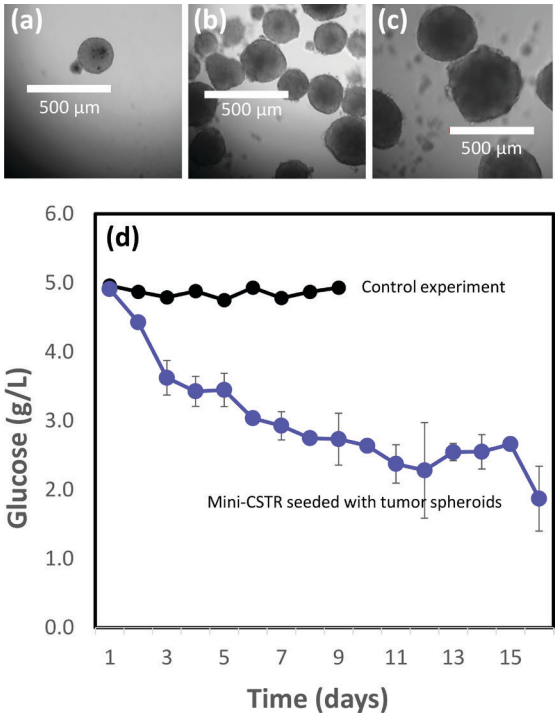

▲ Figure 2: Culture of tumor spheroids by continuous perfusion in this mini-CSTR. (a) Breast cancer tumor spheroids at (a) day 1, (b) day 3, and (c) day 7 of continuous perfusion. (d) The decrease in glucose concentration within the CSTR is an indicator of metabolic activity of the population of spheroids.

FURTHER READING

- D. Bulnes-Abundis, L. M. Carrillo-Cocom, D. Aráiz-Hernández, A. García-Ulloa, M. Granados-Pastor, P. B. Sánchez-Arreola, and M. M. Alvarez, "A Simple Eccentric Stirred Tank mini-Bioreactor: Mixing Characterization and Mammalian Cell Culture Experiments," *Biotechnology and Bioengineering*, vol. 110, pp.1106-1118, 2013.

Chaotic Flows as Micro- and Nanofabrication Tools

G. Trujillo-de Santiago, C. Chávez-Medero, M. Díaz de León-Derby, C. C. Mendoza-Buenrostro, R. F. Martins-Fernandes, M. Samandari, E. González-González, G. Prakash, S. Y. Zhang, A. Khademhosseini, M. M. Alvarez
Sponsorship: MIT-Tecnológico de Monterrey Nanotechnology Program

Nature generates densely packed micro- and nanostructures that enable key functionalities in cells, tissues, and other materials. Current fabrication techniques are far less effective at creating microstructure, due to limitations in resolution and speed. Chaos is one of the many mechanisms that nature exploits to create complexity with simple "protocols." For example, chaotic flows have the extraordinary capacity to create microstructure at an exponential rate. We are currently developing a set of microfabrication strategies that we term chaotic printing—the use of chaotic flows for rapid generation of complex, high-resolution microstructures.

In our experiments, we use two classic mixing systems as models—Journal Bearing (JB) flow and the Kenics mixer—to demonstrate the usefulness of chaotic printing. In a miniaturized JB flow (miniJB), we induced deterministic chaotic flows in viscous liquids (i.e., methacryloyl-gelatin and poly-dimethylsiloxane), and deformed an "ink" (i.e., a drop of a miscible liquid, fluorescent beads, or cells) at an exponential rate to render a densely packed lamellar microstructure that is then preserved by curing or photocrosslinking. In a continuous version of chaotic printing, we created chaotic flows by co-extruding two streams of alginate (two inks) through a printing head that contains an on-line miniaturized Kenics mixer. The result was a continuous 3-D-printing of multi-material lamellar structures with different degrees of surface area and full spatial control of the internal microstructure (Figure 1). The combined outlet stream was then submerged in an aqueous calcium chloride solution to crosslink the emerging alginate fibers containing the microstructure.

The exponentially rapid creation of fine microstructure achievable through chaotic printing exceeds the limits of resolution and speed of the currently available 3-D printing techniques. Moreover, the architecture of the microstructure created with chaotic printing can be predicted using computational fluid dynamic (CFD) techniques. We envision diverse applications for this technology, including the development of densely packed catalytic surfaces and highly complex multi-lamellar and multi-component tissue-like structures for biomedical and electronics applications (Figure 2).

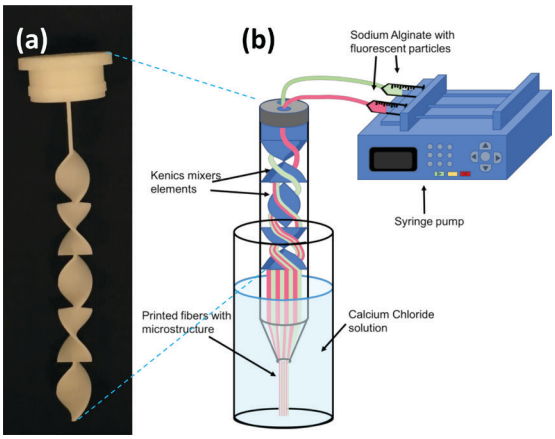

▲ Figure 1: A continuous chaotic printing head based on the use of an on-line Kenics mixer. (a) Details of the mixing head. (b) Schematic representation of the mixing protocol.

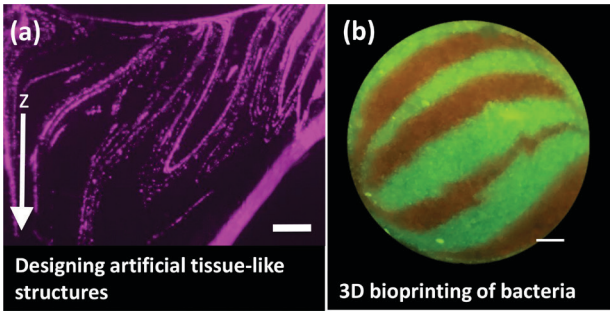

▲ Figure 2: Microfabricating structure using chaotic flows. (a) A tissue-like structure printed by a journal bearing flow. (b) Bioprinting of two types of bacteria in an organized fashion through continuous chaotic printing. Scale bar=500μm.

FURTHER READING

- M. M. Alvarez, F. J. Muzzio, S. Cerbelli, A. Adrover, and M. Giona, "Self-similar Spatiotemporal Structure of Intermaterial Boundaries in Chaotic Flows," *Physical Review Letts.*, vol. 81, pp. 3395-3398, 1998.

On-chip Photonic Aerosol Spectrometer for Detection of Toxic Inhalable Materials

R. Singh, D. Ma, A. Agarwal, B. Anthony

Aerosol particles are distributed in the atmosphere and can constitute serious health threats depending on their chemistry, size, and concentration. For instance, particles of different sizes are deposited in different parts of a lung airway and can lead to specific respiratory complications; and aerosols with certain functional groups can be more harmful than others. So, the comprehensive sensing of aerosol particles is critical for human health, particularly with timely monitoring of environmental pollution, industrial pollution, and defense threats. Most existing aerosol sensors are based on free-space detection methods using optical scattering, IR spectroscopy, and electrical property determination. These sensors can suffer from poor sensitivity and be expensive and bulky.

We have developed an on-chip photonic aerosol spectrometer that can perform *in situ* particle sizing, counting, shape, and chemical characterization. The device is based on an integrated array of waveguide and microresonator structures built on a silicon nitride-on-insulator platform using simple UV photolithography. We have demonstrated that the sensors can estimate the size of particles ranging from 100 nm to 5 microns with particle concentrations over ~500 to 105 particles/cm^3. An aerosol particle falling on the microresonator sensor interacts with the evanescent field of the resonators and acts as a scatterer causing energy loss. The interaction of these particles with the evanescent mode of the microresonators depends on the particle size, shape and count. Coupled with theoretical scattering models of Mie and Rayleigh, we use the measured data to extract physical properties of the airborne particles. The Q-factor of these resonators is as high as 105 enabling sensing resolution to that of an individual aerosol particle. Similarly, by selecting a combination of the resonant wavelengths in microresonators to develop infra-red spectrum sensitive to the distinctive bands of organic and inorganic functional groups inherent in molecularly structures aerosol particles, the spectrometer can be used to do chemical characterization of aerosol particles. This multi resonator platform is tailorable to single or multi-species detection that can be deployed for a variety of aerosol chemistry sensing applications. The technology offers various advantages in particle sensing modalities by offering improved sensitivity, response time and reduced cost and size of the device.

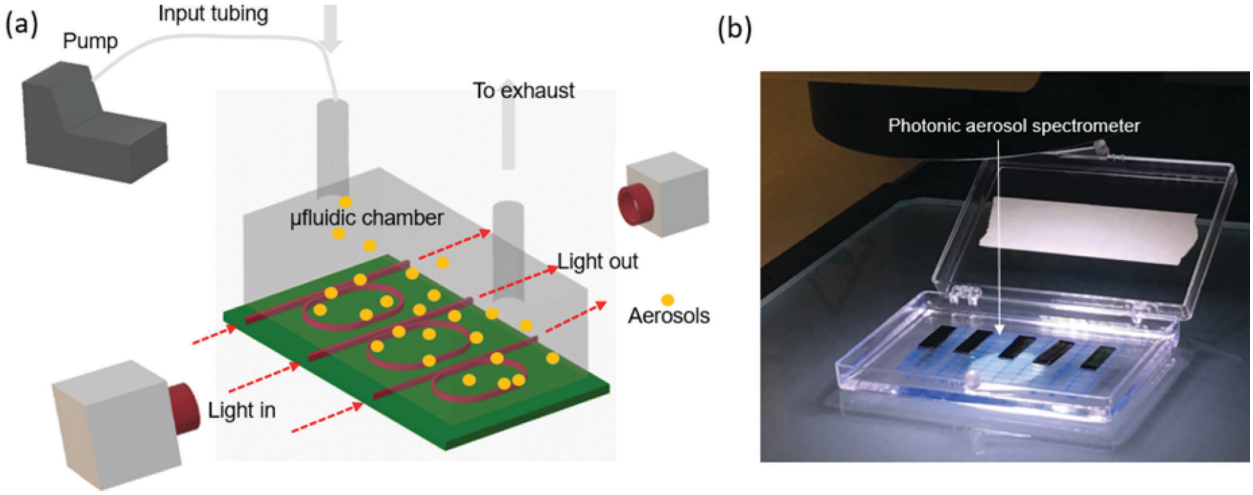

▲ Figure: Schematic of the setup used in on-chip aerosol spectroscopy. It comprises three different parts: namely, aerosol delivery and transport system, on-chip photonic sensing system, and output pattern and spectrum acquisition system. (b) Fabricated photonic aerosol spectrometer.

Close-packed Silicon Microelectrodes for Scalable Spatially Oversampled Neural Recording

J. Scholvin, K. Payer, C. G. Fonstad, E. S. Boyden
Sponsorship: Simons Center for the Social Brain at MIT, Paul Allen Family Foundation, NYSCF, NIH, NSF, CBMM

A major goal of neuroscience is to understand how the activity of individual neurons yields network dynamics, and how network dynamics yields behavior (and causes disease states). Innovative neuro-technologies with orders-of-magnitude improvements over traditional methods are required to reach this goal. Nanofabrication can provide the scalable technology platform necessary to record with single-spike resolution the electrical activity from a large number of individual neurons, in parallel and across different regions of the brain. By combining innovations in fabrication, design, and system integration, we can scale the number of neural recording sites: from traditionally a small number of sparse sites, to currently over 1000 high-density sites, and in the future beyond many thousands of sites distributed through many brain regions.

We designed and implemented close-packed silicon microelectrodes (Figure 1), to enable the spatially oversampled recording of neural activity (Figure 2) in a scalable fashion, using a tight continuum of recording sites along the length of the recording shank, rather than discrete arrangements of tetrode-style pads or widely spaced sites. This arrangement, thus, enables spatial oversampling continuously running down the shank so that sorting of spikes recorded by the densely packed electrodes can be facilitated for all the sites of the probe simultaneously.

We use MEMS microfabrication techniques to create thin recording shanks and a hybrid lithography process that allows a dense array of recording sites which we connect to with submicron dimension wiring. We have performed neural recordings with our probes in the live mammalian brain, and illustrate the spatial oversampling potential of closely packed electrode sites in Figure 2.

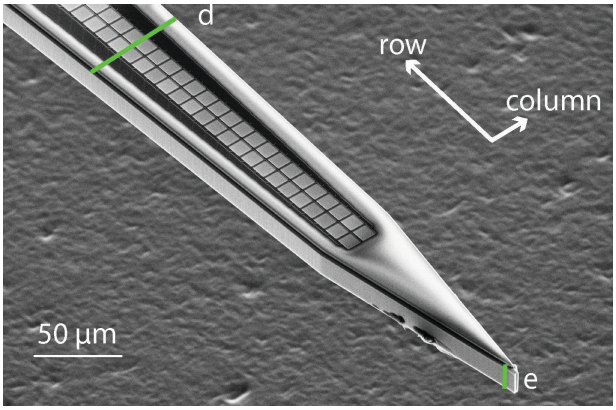

▲ Figure 1: Close-up view of the tip section of a recording shank, showing the two columns and a dense set of rows. The close-packed pads are visible as light squares in the center of the shank. Insulated metal wires connect to the individual sites, running next to the recording sites along the length of the shank; visible as dark lines flanking the rows of light squares. The shank itself has a width of ~50-60 µm in the region shown (d), and is 15 µm thick (e).

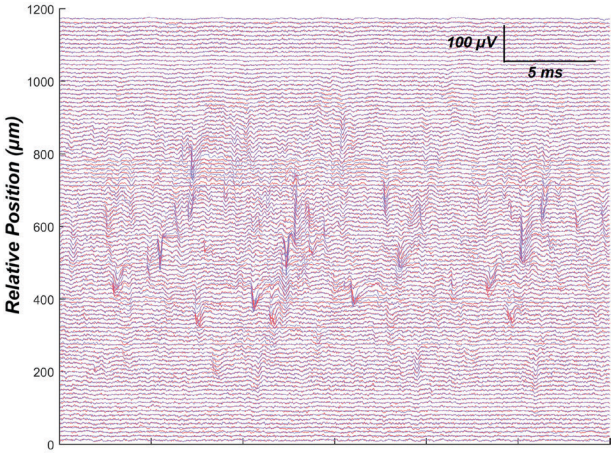

▲ Figure 2: Example of in vivo data from a 2 column by 102 row shank. The spatial oversampling enables spikes to be picked up by many nearby recording sites (9 x 9 µm pads, at a 10.5 µm pitch), to facilitate automated data analysis. The data shown here is a snapshot of data collected by a multi-shank, 1020 channel device.

FURTHER READING

- G. Quadrato, T. Nguyen, E. Macosko, J. Sherwood, S. Yang, D. Berger, N. Maria, J. Scholvin, M. Goldman, J. Kinney, E. Boyden, J. Lichtman, Z. Williams, S. A. McCarroll, and P. Arlotta, "Systems-level Analysis Resolves Cellular Diversity and Neuronal Network Dynamics in Human Brain Organoids," *Nature*, vol. 545 no. 7652, pp. 48-53, 2017.
- J. Scholvin, J. P. Kinney, J. G. Bernstein, C. Moore-Kochlacs, N. Kopell, C. G. Fonstad, and E. S. Boyden, "Close-packed Silicon Microelectrodes for Scalable Spatially Oversampled Neural Recording," *IEEE Trans. Biomed. Eng.*, vol. 63, no. 1, pp. 120–130, 2016.

Building Synthetic Cells for Sensing Applications

M. Hempel, E. McVay, J. Kong, T. Palacios
Sponsorship: AFOSR

Miniaturized sensors, less than 100 µm in diameter, equipped with communication capabilities could enable a new paradigm of sensing in areas such as health care and environmental monitoring. For example, instead of measuring a patient's blood sugar by pricking their finger and analyzing a drop of blood externally, a microscopic sensor in the bloodstream could sense the glucose concentration internally and communicate data to the outside world non-invasively.

In this project, we work towards this vision by integrating chemical sensors and transistors on 100-µm-wide flexible polymer disks that we call synthetic cells or "SynCells" (see Figure 1). The transistor channels and sensors are made of molybdenum disulfide (MoS_2), which it is an excellent material to build digital electronics and highly sensitive sensors. To use the SynCells, they are mixed into a target solution. Upon exposure to a specific substance, the chemical sensors permanently change their electrical resistance. Afterward, the SynCells are retrieved and analyzed externally.

During the last year, we improved our SynCell fabrication process and increased our transistor yield significantly. Furthermore, we successfully demonstrated chemical detection of triethylamine (see Figure 2). As next steps, we want to explore the behavior of our SynCells in microfluidic channels and investigate ways to include time-awareness in these systems.

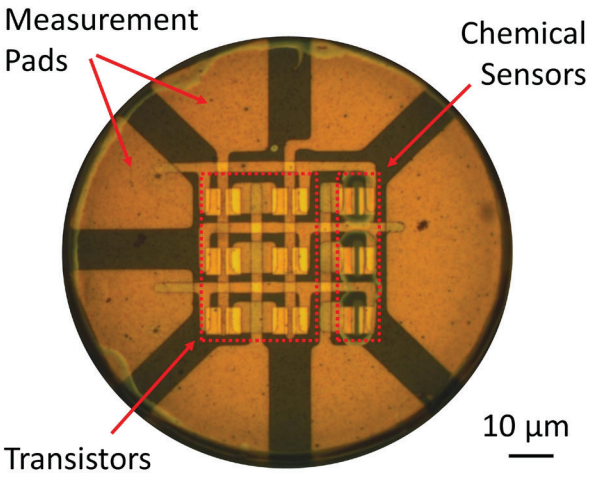

▲ Figure 1: Micrograph of a 100-µm-wide SynCell with three chemical sensors, six transistors, and seven measurement pads.

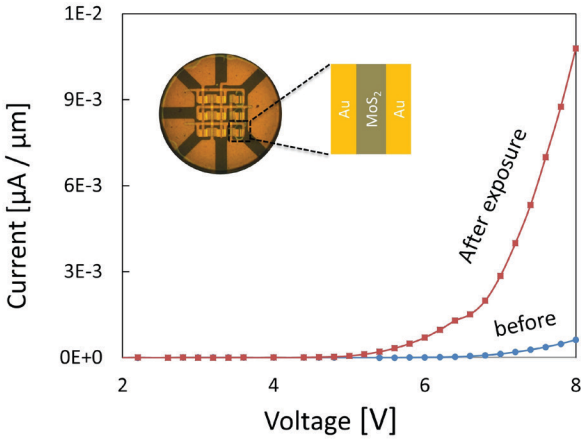

▲ Figure 2: IV-characteristic of a SynCell chemical sensor before and after exposure to triethylamine. The exposure to the toxin permanently increased the sensor's conductance.

FURTHER READING

- L. Yu, et al., "Design, Modeling, and Fabrication of Chemical Vapor Deposition Grown MoS2 Circuits with E-Mode FETs for Large-area Electronics," *Nano Lett.*, vol. 16, no. 10, pp. 6349–6356, Oct. 2016.
- S. S. Varghese, S. H. Varghese, S. Swaminathan, K. K. Singh, and V. Mittal, "Two-dimensional Materials for Sensing: Graphene and Beyond," *Electronics*, vol. 4, no. 3, pp. 651–687, Sep. 2015.
- L. Y. Chen, K. B. Parizi, H. Kosuge, M. Milaninia, M. V. McConnell, H. S. Philip Wong, and A. S. Y. Poon , "Mass Fabrication and Delivery of 3-D Multilayer µTags into Living Cells," *Scientific Reports*, vol. 3, pp. 2295, Jul. 2013.

The AutoScope: An Automated Point-of-Care Urinalysis System

S. R. Primas, C. G. Sodini
Sponsorship: MEDRC - Analog Devices, Inc.

Urinalysis is one of the most common diagnostic techniques in medicine. Over 200 million urine tests are ordered each year in the US, costing between $800 to $2,000 million in direct costs. 46% of all urinalysis tests include microscopic analysis, which involves identifying and counting each particle found in the urine. Microscopic urinalysis is a costly and complex process often done in medical laboratories. An inexpensive and automated cell-counting system would (1) increase access to microscopic urinalysis and (2) shorten the turn-around time for physicians to make diagnostic decisions by permitting the test to be done at the point-of-care.

The AutoScope is an automated, low-cost microscopic urinalysis system that can accurately detect red blood cells (RBCs), white blood cells (WBCs), and other particles in urine. We use a low-cost image acquisition system combined with two neural networks to identify these particles. By not using any optical magnification, we achieve costs three orders of magnitude less than the only commercially available semi-automated urinalysis system and a device size of 8.3 x 6.0 x 8.8cm.

To validate the system, we calculated the accuracy, sensitivity, and specificity of the Autoscope. The specificity and sensitivity were determined by generating 209 digital urine specimens modeled after urine received in medical labs. The Autoscope had a sensitivity of 88% and 91% and a specificity of 89% and 97% for RBCs and WBCs, respectively. Next, we determined the Autoscope's accuracy by fabricating 8 synthetic urine samples with RBCs, WBCs, and microbeads. The reference results were confirmed through a medical laboratory. The AutoScope's counts and the reference counts were linearly correlated to each other (r^2= 0.980) across all particles. The sensitivity, specificity, and R-squared values for the AutoScope are comparable (and mostly better) than the same metrics for the iQ-200, a $100,000-$150,000 state-of-the-art semi-automated urinalysis system.

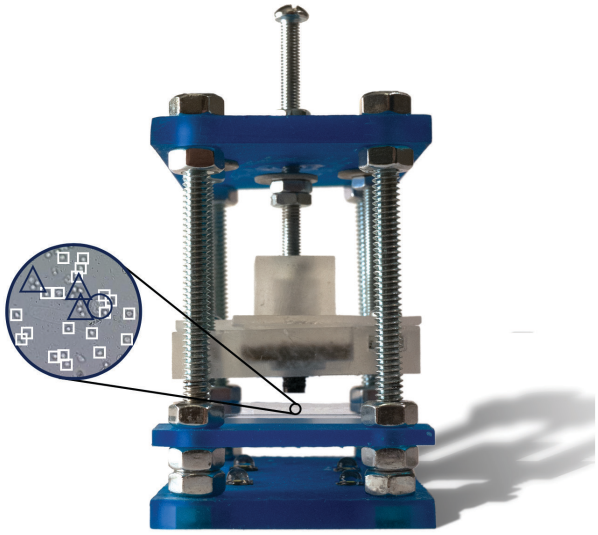

▲ Figure 1: A side-view of the AutoScope system. The cost of the bill-of-materials is $57-$92. The end-to-end resolution is 5.86-8.29um.

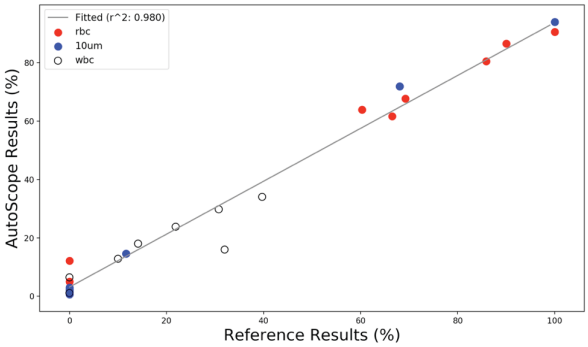

▲ Figure 2: The end-to-end accuracy of the fully-automated AutoScope system (with an R-squared of 0.980). Reference results were cross-validated by a medical laboratory.

FURTHER READING

- M. Ranzato, et al., "Automatic Recognition of Biological Particles in Microscopic Images," *Pattern Recognition Letts.*, 28.1, pp. 31-39, 2017.
- N. A. Switz, M. V. D'Ambrosio, and D. A. Fletcher, "Low-cost Mobile Phone Microscopy with a Reversed Mobile Phone Camera Lens," *PloS one* 9.5, e95330, 2014.

Cardiac Output Measurement using Ballistocardiography and Electrocardiography

K. Beeks, C. G. Sodini
Sponsorship: MEDRC – Analog Devices, Inc.

Cardiac output (CO) is one of several parameters used by cardiologists to stratify risk of patients with cardiovascular disease and has significant clinical relevance. CO is currently obtained in the ICU setting through right heart catheterization, an invasive method. This kind of procedure brings with it increased financial cost and risk to the patient. Consequently, non-invasive methods, such as ballistocardiography (BCG), have been gaining more traction and are seen as potential candidates for measuring cardiovascular parameters such as CO.

BCG utilizes detection of the body's recoil from the ejection of blood into the arterial system. Due to its nature, BCG is prone to noise and ensemble averaging of multiple cardiac cycles is used to obtain a waveform with higher signal-to-noise ratio. An electrocardiogram (ECG) handlebar is used to generate the ECG waveform that sets the timing of the cardiac cycles for this technique. The most notable features of the BCG waveform (I, J, and K waves) are driven by the difference in blood pressure between the inlet and outlet of the ascending aorta during a cardiac cycle. Several parameters derived from these features in the waveform, such as I-J amplitude, IJK width, and the R-J interval, can be used to determine a patient's stroke volume. Once the stroke volume is known, it can be used alongside the heart rate to calculate the cardiac output. This kind of device can be used for continuous monitoring of a patient in the home setting, removing many of the limitations seen with invasive methods.

▲ Figure 1: The device shown here is used to generate the BCG waveform. The scale contains the force sensor and the handlebar uses electrocardiography and is used to help process the BCG signal.

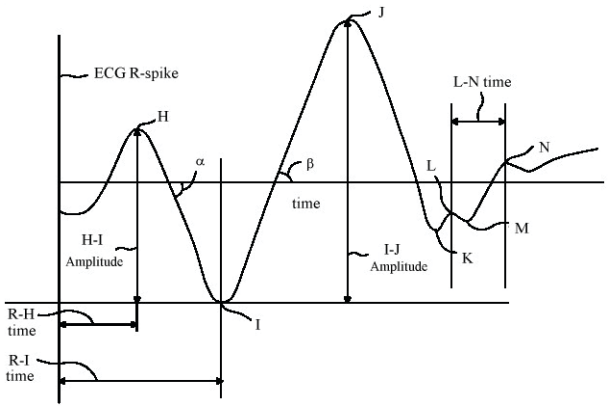

▲ Figure 2: The typical BCG waveform has multiple features but, the most useful are the I, J, and K waves. Parameters derived from these waves are especially useful in finding stroke volume.

FURTHER READING

- H. Ashouri, L. Orlandic, and O. T. Inan, "Unobtrusive Estimation of Cardiac Contractility and Stroke Volume Changes using Ballistocardiogram Measurements on a High Bandwidth Force Plate," *Sensors (Basel, Switzerland)*, vol. 16, no. 6, pp. 787, http://doi.org/10.3390/s16060787F, 2016.
- C.-S. Kim, S. L. Ober, M. S. McMurtry, B. A. Finegan, O. T. Inan, R. Mukkamala, and J.-O. Hahn, "Ballistocardiogram: Mechanism and Potential for Unobtrusive Cardiovascular Health Monitoring," *Scientific Reports*, vol. 6, pp. 31297, http://doi.org/10.1038/srep31297, 2016.
- L. Giovangrandi, O. T. Inan, R. M. Wiard, M. Etemadi, and G. T. A. Kovacs, "Ballistocardiography – A Method Worth Revisiting," *Conference Proceedings: Annual International Conference of the IEEE Engineering in Medicine and Biology Society, IEEE Engineering in Medicine and Biology Society, Annual Conference,* pp. 4279–4282, 2011.

Continuous and Non-invasive Arterial Pressure Waveform Monitoring using Ultrasound

J. Seo, H.-S. Lee, C. G. Sodini
Sponsorship: MEDRC – Philips, CICS

An arterial blood pressure (ABP) waveform provides valuable information for understanding cardiovascular diseases. The ABP waveform is usually obtained through an arterial line (A-line) in intensive care settings. Although considered the gold standard, the disadvantage of this method is its invasive nature. Non-invasive methods such as vascular unloading and tonometry are not suitable for prolonged monitoring. Therefore, reliable non-invasive ABP waveform estimation has long been desired by medical communities. Medical ultrasound is an attractive imaging modality because it is inexpensive, cuff-less, and suitable for portable system implementation.

The proposed ultrasonic ABP waveform monitoring is achieved by ultrasonography to observe the pulsatile change of the cross-sectional area and identify the vessel elasticity, represented by the pulse wave velocity (PWV); the propagation speed of a pressure wave along an arterial tree) with a diastolic pressure measurement. The local PWV can be estimated from the flow-area plot during a reflection-free period (e.g., the early systolic stage).

A prototype ultrasound device was designed to conduct application-specific ultrasonography in a portable form factor, shown in Figure 1. The first human subject validation shows the agreement between this method on the common carotid artery and the ABP waveform obtained at a middle finger using the vascular unloading method. Motion-tolerant ultrasonography is explored to improve the measurement stability from the first design for long term monitoring. The second human subject study in a transient stress situation demonstrates the proof-of-concept of this method for the stress testing. Currently, the human subject study to compare the A-line with this method in collaboration with Boston Medical Center is in progress.

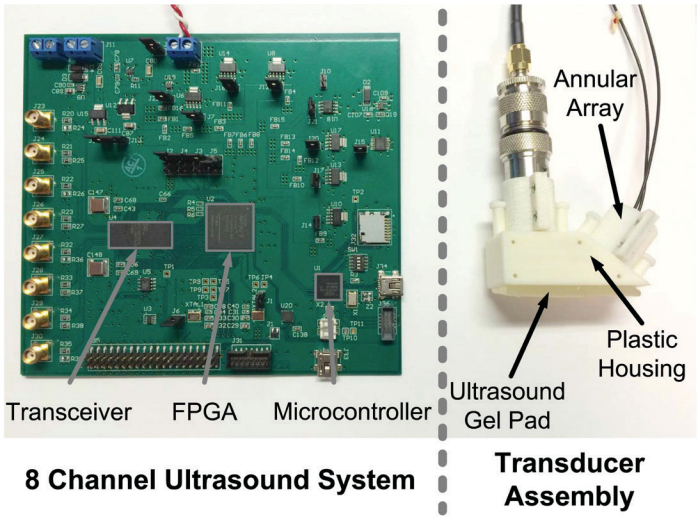

▲ Figure 1: The prototype ultrasound system and transducer assembly. The system is capable of sufficient data rate to display blood flow and arterial pulsation simultaneously. Ultrasound gel pad is utilized to achieve acoustic coupling between the transducer surface and the skin.

▲ Figure 2: Application of the probe for motion-tolerant ultrasonography. This probe is manually held or secured by rubber bands around the subjects' neck for the human study in a transient stress situation.

FURTHER READING

- J. Seo, S. J. Pietrangelo, C. G. Sodini, and H.-S. Lee, "Motion Tolerant Unfocused Imaging of Physiological Waveforms for Blood Pressure Waveform Estimation using Ultrasound" *IEEE Transactions on Ultrasonics, Ferroelectrics, and Frequency Control*, vol. 65, no. 5, pp. 766-779, Mar. 2018.
- J. Seo, S. J. Pietrangelo, H.-S. Lee, and C. G. Sodini, "Carotid Arterial Blood Pressure Waveform Monitoring using a Portable Ultrasound System," *2015 37th Annual International Conference of the IEEE Engineering in Medicine and Biology Society (EMBC)*, pp. 5692-5695, Aug. 2015.

Breathable Electronic Skin Sensor Array through All-in-One Device Transfer

H.-W. Yeon, P. Lin, S. Bae, B. Lee, S. Ryu, J. Kim
Sponsorship: AMOREPACIFIC

Skin electronics, which can laminate on human skin, have emerged as essential tools for human/Internet of things (IoTs) interfaces such as real-time health monitoring and instantaneous medical treatment. Amid this sweeping trend, human skin has been treated as merely a flexible, stretchable, and soft space for mounting of skin electronic devices. The skin is the outmost and the largest organ covering the external body surface and plays a vital role to maintain human life. Thus, homeostasis of the skin should be maintained even beneath the electronics. However, conventional thin-film device design, neglecting the skin, can induce problems (e.g., inflammation).

Here we propose a breathable skin electronics, not blocking physiological activity of the skin. Sweat pore-inspired micro-hole pattern in a skin patch secure ~100% breathability and an elastic modulus of the skin patch has comparable value of the skin, which can replicate mechanical deformation of the skin with strong adhesion.

Furthermore, we develop all-in-one device transfer process that high-temperature processed (~500 ˚C), photo-patterned inorganic device array is directly transferred onto the skin patch (Figure 1). High-quality inorganic semiconductors on skin-like patch lead to highly sensitive electromechanical devices such as strain sensors (Figure 2).

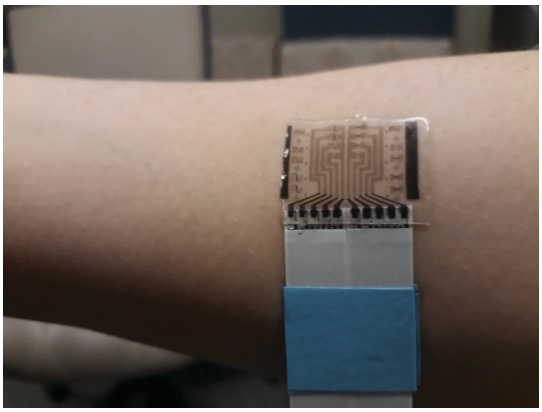

▲ Figure 1: Skin sensor array with an external wire through all-in-one device transfer.

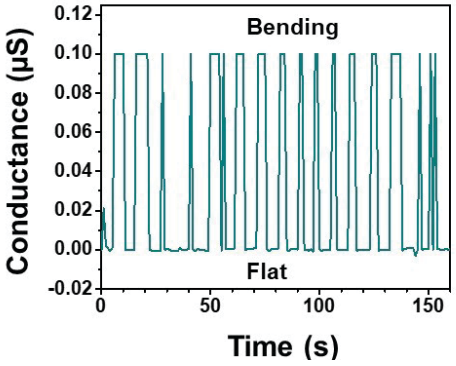

▲ Figure 2: Piezoelectric sensor. Conductance changes as a function of compressive bending stress.

Secure System for Implantable Drug Delivery

S. Maji, U. Banerjee, R. T. Yazicigil, S. H. Fuller, A. P. Chandrakasan
Sponsorship: Analog Devices, Inc., Fellowship

Recent years have witnessed a growing increase in the use of implantable and wearable medical devices for monitoring, diagnosing, and treating our medical conditions. Advancements in electronics have opened up new avenues for deploying these devices towards applications previously overlooked, such as implanting an entire repository of a medical drugs within the human body for effective time-released delivery. The advantages of a time-released implant offer over some conventional oral dosage forms are site-specific drug administration for targeted action, minimal side-effects, and sustained release of therapeutic agent. Patient compliance is more positive with the treatment regimen associated with an implantable device as it is considerably less burdensome than pills or injections. The prominent application for implantable drug delivery includes diabetes management, contraception, HIV/AIDS prevention, and chronic pain management.

In many of these applications, the control of the command to these devices lies with the patient, who can program the device as needed. For example, a woman can program her monthly schedule of contraception for her family planning and allow the device to release regular doses of contraception, alleviating daily doses. However, an alarming concern that is associated with it is the generic security concerns with regular IoT devices, and potentially, with much more catastrophic effects. Any compromise of the controller device/cell phone would render the system ineffective. The fact that there is no direct feedback from the implantable to the patient makes it even more difficult. A simple example is a malicious cell-phone continuously commanding the device to release drug without the knowledge of patient.

Our work focusses on solving this problem with a combination of energy-efficient cryptography with relevant physiological properties of the user. This makes it very difficult for any attacker, even with significant control over the controller, to break the system, while providing legitimate feedback to the user.

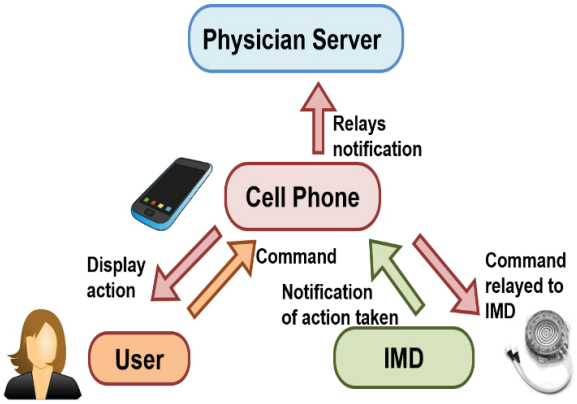

▲Figure 1: A generic diagram of an implantable drug delivery system involving all the parties.

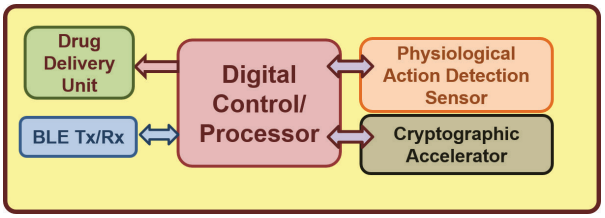

▲Figure 2: Components of the proposed secure implantable drug-delivery system.

FURTHER READING

- P. Nadeau, "Ultra-low Energy Electronics for Synthetic Biological Sensors," *Ph.D. Thesis,* MIT, Sep. 2016.
- M. Zhang, A. Raghunathan, and N. K. Jha, "Trustworthiness of Medical Devices and Body Area Networks," *Proceedings of the IEEE,* vol. 102, no. 8, pp. 1174–1188, Aug. 2014.

Enabling Saccade Latency Measurements with Consumer-grade Cameras for Monitoring of Neurodegenerative Disease Progression

H.-Y. Lai, G. Saavedra-Peña, T. Heldt, V. Sze

Quantitative and accurate tracking of neurodegenerative disease remains an ongoing challenge. Diagnosis requires patients to undergo time-consuming neuropsychological tests that suffer from high-retest variability, making it difficult to assess the progression of the disease or a patient's response to experimental treatments.

We tackle the lack of an objective measurement to track the progression of neurodegenerative diseases by designing algorithms that can quantify subtle changes across time in eye movement patterns that correlate with disease progression. One such feature is saccade latency – the time delay between the appearance of a visual stimulus and when the eye starts to move towards said stimulus. As a result, an unobtrusive tool that measures saccade latency (or other metrics of eye movement) consistently across time can enable the quantification of disease progression and the assessment of a patient's response to treatment.

We propose a pipeline (Figure 1) to modify and evaluate a set of candidate eye-tracking algorithms to operate on video sequences obtained from an iPhone 6, for accurate and robust determination of saccade latency. A variant of the iTracker algorithm performed most robustly and resulted in mean saccade latencies and associated standard deviations on iPhone recordings that were essentially the same as those obtained from recordings using a high-end, high-speed camera (Figure 2). Our results suggest that accurate and robust saccade latency determination is feasible using consumer-grade cameras and might, therefore, enable unobtrusive tracking of neurodegenerative disease progression.

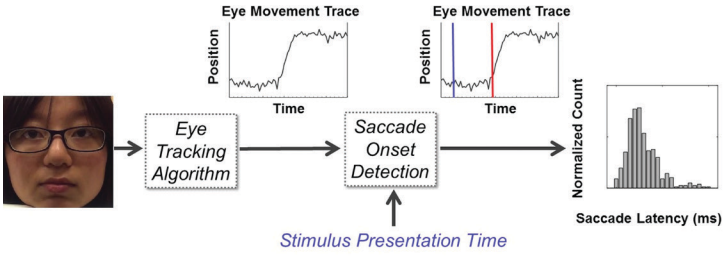

▲ Figure 1: Pipeline for eye-tracking algorithm evaluation. An iPhone 6 video is processed by an eye tracking algorithm. Saccade latency values are calculated from the eye movement trace obtained with the algorithm.

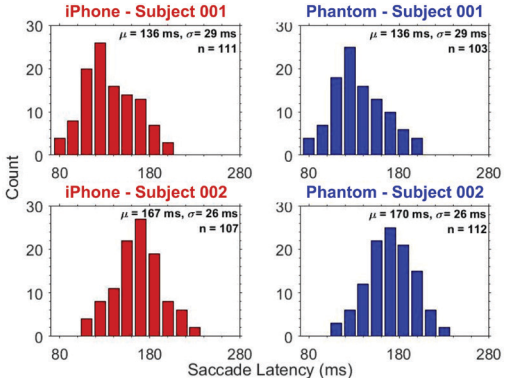

▲ Figure 2: Saccade latency histograms, from two different subjects, obtained from simultaneous recordings of an iPhone 6 (left) and a research-grade camera (right). Notice the similarity between distributions across recording platforms.

FURTHER READING

- H.-Y. Lai, G. Saavedra-Peña, C. Sodini, T. Heldt, and V. Sze, "Enabling Saccade Latency Measurements with Consumer-grade Cameras for Monitoring of Neurodegenerative Disease Progression," *Proceedings of the IEEE International Conference on Image Processing (ICIP)*, 2018.
- G. Saavedra-Peña, H.-Y. Lai, V. Sze, and T. Heldt "Determination of Saccade Latency Distributions using Video Recordings from Consumer-grade Devices," *Proceedings of the IEEE Engineering in Medicine and Biology Conference (EMBC)*, 2018.
- K. Krafka, A. Khosla, P. Kellnhofer, H. Kannan, S. Bhandarkar, W. Matusik, and A. Torralba, "Eye Tracking for Everyone," *IEEE Conference on Computer Vision and Pattern Recognition (CVPR)*, 2016.
- R. Shafiq-Antonacci, P. Maruff, C. Masters, and J. Currie, "Spectrum of Saccade System Function in Alzheimer's Disease," *Archives of Neurology*, vol. 60, pp. 1275–1278, 2003.